Journal of Biomolecular NMR, **26:** 157–166, 2003.
KLUWER/ESCOM
© 2003 *Kluwer Academic Publishers. Printed in the Netherlands.*

Multiple quadrature detection in reduced dimensionality experiments

Wiktor Koźmiński[a,*] & Igor Zhukov[b]
[a]*Department of Chemistry, Warsaw University, ul. Pasteura 1, 02-093 Warszawa, Poland;* [b]*Institute of Biochemistry and Biophysics, Polish Academy of Sciences, ul. Pawińskiego 5a, 02106 Warszawa, Poland*

Received 15 January 2003; Accepted 14 February 2003

Key words: HACANH, HNCA, HN(CO)CA, reduced dimensionality, sequential assignment, triple resonance, ubiquitin

Abstract

A new, simple procedure is proposed which enables acquisition of two or more chemical shifts encoded in a common dimension simultaneously in quadrature. For n chemical shifts projected in a single dimension, the expected effect is obtained by interleaved acquisition and appropriate combination of 2^n data sets per increment of respective evolution time. The particular chemical shifts can be calculated from sums and differences of signal frequencies obtained by different combination of the acquired data sets. In comparison to the established reduced dimensionality (RD) techniques, the proposed method enhances resolution due to reduction of the number of signals and requires less evolution time increments owing to narrower spectral width in the RD-domain. We show examples of the application of the new approach to the 2D HNCA and HN(CO)CA techniques with two, and 2D HACANH with three frequencies simultaneously encoded in the t_1 evolution period, for ^{13}C,^{15}N-labeled ubiquitin.

Introduction

The conventional strategy of NMR based protein structure determination was enabled by the application of ^{1}H homonuclear 2D NMR experiments (Wüthrich, 1986). A significant extension of this procedure has been achieved due to the availability of ^{13}C, ^{15}N enriched proteins by introduction of triple-resonance three- or four-dimensional experiments (Montelione and Wagner, 1989; Ikura et al., 1990; Bax and Grzesiek, 1993; Yamazaki et al., 1994). These recently reviewed techniques (Sattler et al., 1999) utilize scalar couplings for polarization transfers and enable one to assign all backbone ^{1}H, ^{13}C and ^{15}N resonances.

The acquisition of 3D or 4D data sets allows one to correlate three or four different chemical shifts, respectively, and to separate degenerated signals by spreading them in different frequency domains. The obtainable digital resolution is however strongly limited by the acceptable experimental time. The most important source of this limitation, directly relating the experiment time and achievable resolution, is the necessity of acquisition of a large quantity of data sets, proportional to the product of the number of points in all indirectly detected time domains.

A promising solution of this problems was the idea of Reduced Dimensionality (RD) experiments (Szyperski et al., 1993a, 1993b, 1994, 1995, 1996, 1997, 1998; Brutscher et al., 1994, 1995; Löhr and Ruterjans, 1995). These methods, analogously to the concept of Accordion Spectroscopy (Bodenhausen and Ernst, 1981, 1982), employ simultaneous sampling of two chemical shifts evolutions. Thus, the N chemical shifts could be effectively encoded in the resulting $(N-1)$-dimensional spectrum with the advantage of shorter experimental time and with digital resolution typical for the $(N-1)$D spectra. Recently, it was also shown that such a technique could be applied for incorporating three different frequencies in a single domain, hence a reduction of dimensionality from ND to $(N-2)$D (Ding and Gronenborn, 2002) was obtained. In these cases, except for the recently published 3D HNN[CAHA] and 3D HNN(CO)[CAHA] techniques (Xia et al., 2002), quadrature detection was

*To whom correspondence should be addressed. E-mail: kozmin@chem.uw.edu.pl

employed for only one of the chemical shifts. The successive simultaneously sampled frequencies simply introduced a cosine-type amplitude modulation in the time domain and consequently doubling of signals in the frequency domain was observed, with the apparent separation equal to twice the rotating-frame frequency of the respective nuclei.

The lack of quadrature for all of the simultaneously sampled frequencies in most of the so far proposed RD-techniques leads to two significant drawbacks of the latter. First, the number of peaks is doubled for each additional frequency in the common dimension, which unnecessarily complicates spectra and may introduce peak overlap. And second, the frequency offset for the nuclei detected without quadrature should be set outside of the spectral region of interest owing to the impossibility of defining the sign of the frequencies, which forces one to increase the spectral width in the RD-domain and accordingly increases the number of evolution time increments necessary to obtain the required maximum evolution time. The TPPI method can be applied in order to obtain artificial frequency offsets (Ding and Gronenborn, 2002; Xia et al., 2002). This approach is helpful in separating different kinds of cross-peaks, however, at the expense of a further increase of the spectral width in the RD-domain. Although simultaneous quadrature for H_α and C_α frequencies was recently proposed (Xia et al., 2002), the described method involves a number of pulses and appears not to be generally applicable.

In this work we propose a simple and general method for multiple simultaneous quadrature detection with preservation of purely absorptive line-shape. The expected effect is achieved by a straightforward extension of known rules of quadrature detection. For n frequencies in a common domain the acquisition and appropriate combination of 2^n FIDs per each t_1 increment is necessary. These data sets collected in interleaved mode should consist of all possible combinations of sine and cosine modulation. The new technique is applicable to any ND experiment ($N > 2$), where it is possible to detect each single frequency in quadrature. Additionally, the same procedure is appropriate to separate single-quantum frequencies in multiple-quantum evolution periods. In most cases the expected effect could be obtained by simple modifications of the existing pulse sequence codes.

Methods

In the case of single frequency ($n = 1$) the standard States (States et al., 1982) or States-TPPI (Marion et al., 1989), procedures to obtain quadrature detection and pure absorption line-shapes are the methods of choice. In both cases, recording of the two amplitude modulated data sets, $\cos(\Omega t_1)$ and $\sin(\Omega t_1)$, which form the real and imaginary parts of the t_1 interferogram, respectively, is required. However, in the case of phase modulation in t_1, which is usually obtained using gradient echo- and anti-echo coherence selection, in sensitivity enhanced sequences (Palmer III et al., 1991; Kay et al., 1992; Sattler et al., 1995) or TROSY (Pervushin et al., 1997; Weigelt, 1998) experiments, the amplitude modulation should be reestablished prior to Fourier transformation. The $\cos(\Omega t_1)$ and $\sin(\Omega t_1)$ amplitude modulated interferograms are calculated as the sum and difference of echo- and anti-echo data sets, respectively, followed by $\pi/2$ phase correction along the directly detected time domain, of the second one.

For the two frequencies of spins A and B, sampled simultaneously, i.e., $n = 2$, the following four data sets should be generated:
(1) $\cos(\Omega_A t_1)\cos(\Omega_B t_1)$,
(2) $\sin(\Omega_A t_1)\cos(\Omega_B t_1)$,
(3) $\cos(\Omega_A t_1)\sin(\Omega_B t_1)$,
(4) $\sin(\Omega_A t_1)\sin(\Omega_B t_1)$.

Conventional Fourier transformation of pairs (1, 2) and (3, 4) produces two different spectra with quadrature for spin A, modulated by $\cos(\Omega_B t_1)$ and $\sin(\Omega_B t_1)$, respectively. The first consists of in-phase, while the second, after $\pi/2$ phase correction in t_1, of the anti-phase doublets along the F_1 dimension, with splittings equal to $2\Omega_B$. Thus, addition of $\pi/2$ phase corrected pair (3, 4) to (1, 2) generates the spectrum with cross-peak frequencies of $\Omega_A + \Omega_B$, whereas its substraction – of $\Omega_A - \Omega_B$, in the F_1 dimension, respectively. Analogously, simply by negating the respective imaginary contributions, quadrature image spectra, i.e., ones consisting of peaks at $-\Omega_A - \Omega_B$, and $-\Omega_A + \Omega_B$ frequencies, could be created. However, only the pair of spectra with opposite signs of one of the frequencies, is independent and should be considered. The equivalent technique was described for determination of one-bond ^{15}N-^{1}H couplings and referred to as IPAP (In-Phase – AntiPhase) (Ottiger et al., 1998). In this case Ω_A and Ω_B were $\Omega(^{15}N)$ and πJ, respectively. The ^{15}N quadrature was obtained conventionally in States-TPPI manner, whereas

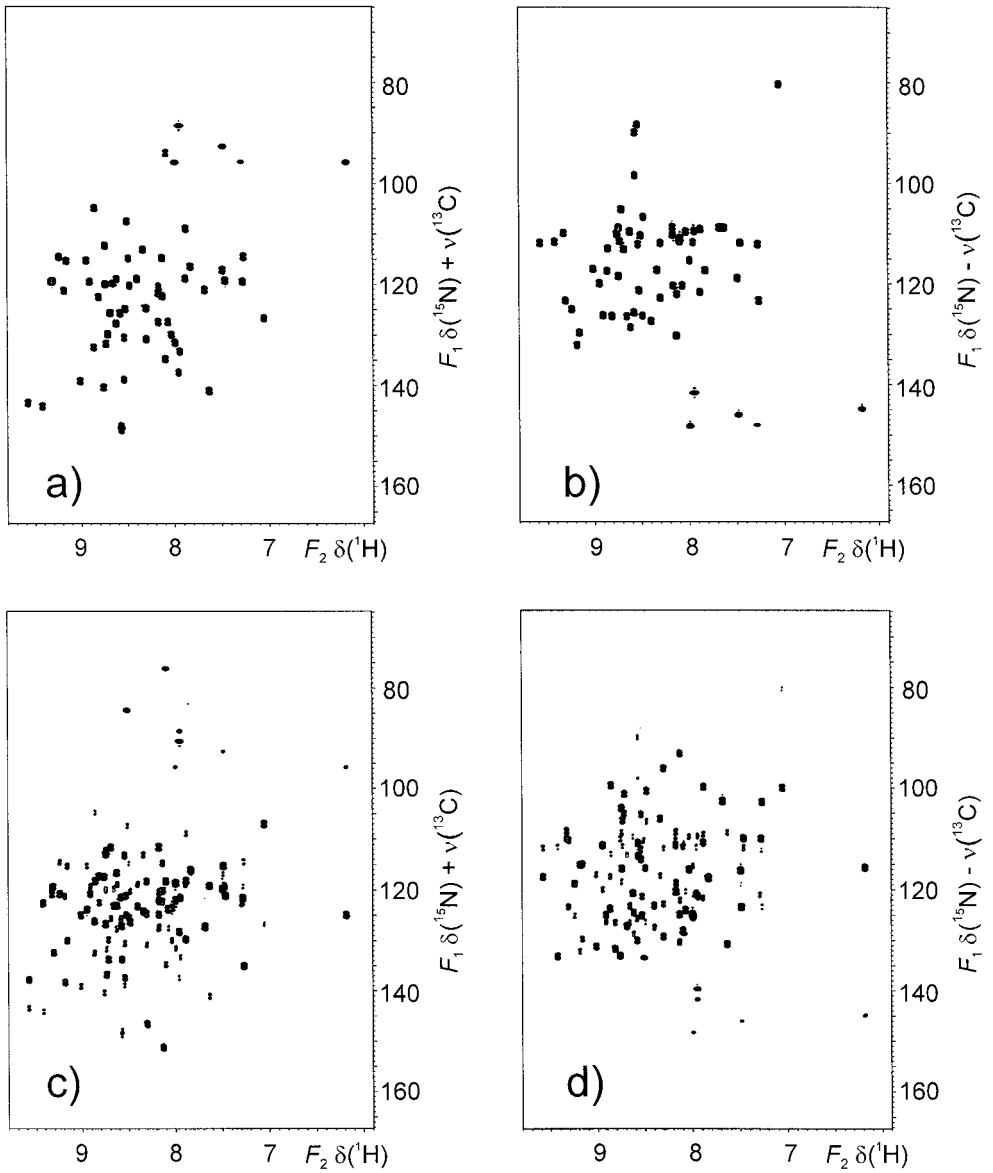

Figure 1. Two-dimensional spectra obtained using reduced dimensionality 2D HN(CO)CA (a and b) and 2D HNCA (c and d) experiments applied for ^{13}C, ^{15}N-labeled ubiquitin sample. The time-domain data was processed, according to Table 1, to obtain cross-peak frequencies at $\delta(^{15}N) + \nu(^{13}C)$ and $\delta(^{15}N) - \nu(^{13}C)$, (a and c) and (b and d), respectively. 16 scans were coherently added for each data set for 145 t_1 increments. The maximum t_1 and t_2 times were 27.9 and 85 ms, respectively. The spectral width of 5200 Hz, covering the sum of ^{15}N and $^{13}C_\alpha$ spectral ranges, was set for the F_1 dimension. A relaxation delay of 1.5 s was used. The data matrix containing 145 × 512 complex points in t_1 and t_2 respectively, was zero-filled to 512 × 1024 complex points, cosine weighting function was applied prior to Fourier transformation in both dimensions.

$\sin(\pi J t_1)$ modulation was chosen by insertion of an additional $(2J)^{-1}$ coupling evolution period.

The same procedure could be further extended for simultaneous labeling of any number (n) of chemical shifts in a common dimension. However, sampling of each additional evolution doubles the number of required data sets owing to the necessity of recording both sine and cosine modulated interferograms.

The number of necessary data sets increases analogously to conventional ND experiments, were also a 2^{N-1} data sets should be collected for each (t_1, …, t_{N-1}) point in order to obtain pure absorption line-shapes. Therefore, the measurement time of pro-

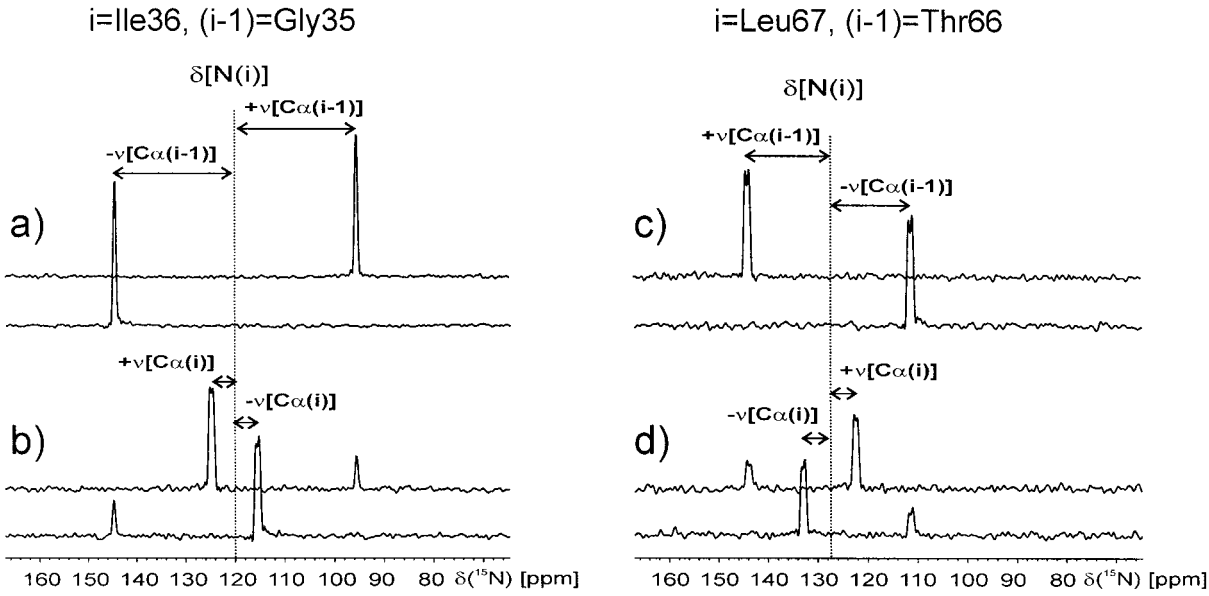

Figure 2. Comparison of the F_1 cross sections across amide resonances of Ile36 (a, b) and Leu67 (c, d) residues obtained from the spectra given in Figure 1. (a, c) 2D HN(CO)CA and (b, d) 2D HNCA experiments. In each pair, in upper spectrum ^{13}C frequencies are positive in relation to carrier frequency. The dotted lines denote the ^{15}N chemical shift and arrows the relative $^{13}C_\alpha$ frequencies.

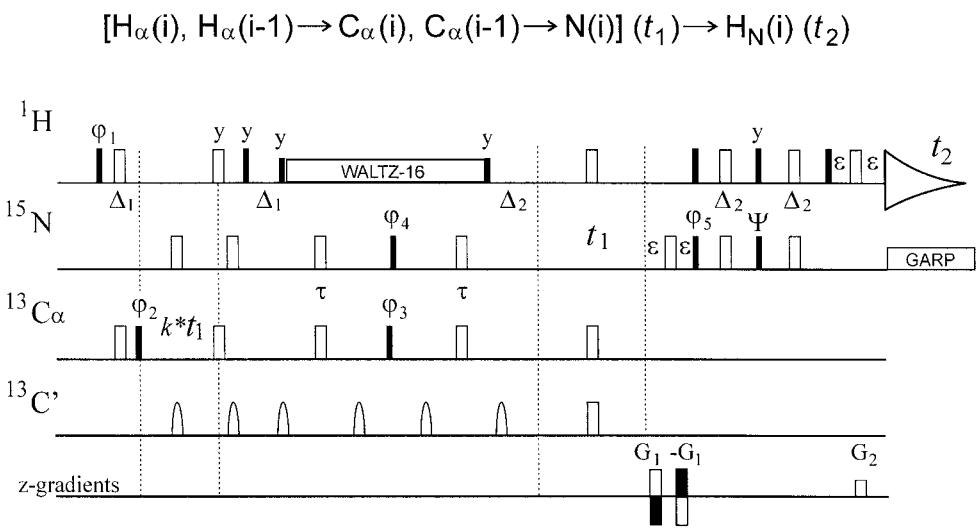

Figure 3. Pulse sequence of the reduced dimensionality 2D HACANH experiment. Dark-filled and open bars represent $\pi/2$ and π pulses, respectively. All pulses are applied along the rotating-frame x-axis unless indicated differently. The selective inversion C' π-pulses are applied in pairs to avoid Bloch-Siegert phase shifts. The delays Δ_1 and Δ_2 should be tuned to $0.5/^1J(^{13}C, ^1H)$ and $0.5/^1J(^{15}N, ^1H)$, respectively. τ (28,6 ms) was optimized for maximum amplitude of polarization transfer between C_α and N. ε includes the rectangular – shaped gradient pulse and a 100 μs recovery time. The k factor enables relative scaling of the t_1 increments in both evolution periods, thus maximum possible t_1 can be optimized with respect to effective relaxation rates and the expected spectral resolution. The basic phase cycle is: $\varphi_1 = 4x,4(-x)$, $\varphi_2 = x,-x$, $\varphi_3 = 8x,8(-x)$, $\varphi_4 = 2x,2(-x)$, $\varphi_5 = 16x, 16(-x)$ and $\varphi_R = x, 2(-x), x, 2(-x, 2x, -x), x, 2(-x), x, -x, 2x, -x, 2(x, 2(-x), x), -x, 2x, -x$. Gradients G_1 and G_2 with a duration of 1 ms and the relative amplitude of $\pm 0.5\ \gamma_H/\gamma_N$, were used for echo-antiecho selection. Additionally, the sensitivity-enhancement scheme requires phase ψ to be set to $\varphi_5 - \pi/2$ in echo and $\varphi_5 + \pi/2$ in antiecho experiments, respectively. The ^1H and ^{13}C quadrature could be obtained by $\pi/2$ phase shifts of φ_1 and φ_2, respectively. The axial peaks are displaced by reversing of sign of φ_1 and receiver phase (φ_R) for the even t_1 increments. The quadrature detection for all three chemical shifts labeled in t_1 requires acquisition of the eight data sets per each t_1 increment, consisting the combinations of echo and antiecho selection for ^{15}N with the phases φ_1 and φ_2 set to x and y.

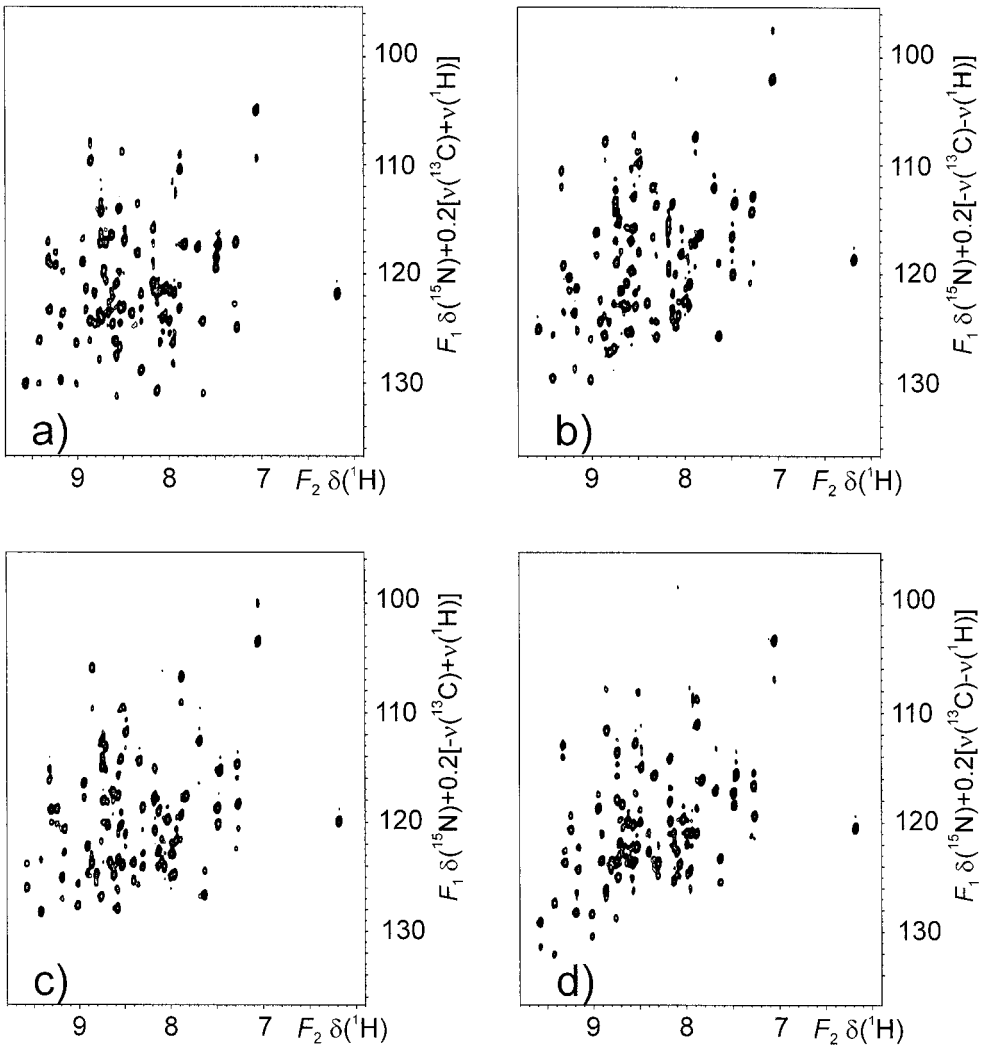

Figure 4. Contour plots obtained by application of the 2D HACANH pulse sequence from Figure 3 to ^{13}C, ^{15}N-labeled ubiquitin sample. The $^{13}C_\alpha$ and $^1H_\alpha$ frequencies were scaled down using k factor set to 0.2. The data was processed with retention of correct ^{15}N frequency (a) All three ^{15}N, $^{13}C_\alpha$ and $^1H_\alpha$ frequencies positive, (b) $^{13}C_\alpha$ and $^1H_\alpha$ negative (c) $^{13}C_\alpha$ negative and (d) $^1H_\alpha$ negative. 64 scans were coherently added for each data set for 180 t_1 increments. The maximum t_1 and t_2 times were 85.7 and 85 ms, respectively. The spectral width of 2100 Hz, covering the sum of ^{15}N, $^{13}C_\alpha$ and $^1H_\alpha$ spectral ranges (considering scaled of $^{13}C_\alpha$ and $^1H_\alpha$ frequencies) was set for the F_1 dimension. A relaxation delay of 1.4 s was used. The data matrix containing 180 × 512 complex points in t_1 and t_2, respectively, was zero-filled to 512 × 1024 complex points, cosine square weighting function was applied prior to Fourier transformation in both dimensions.

posed experiment is reduced by a factor proportional to product of number of evolution time points to be sampled in t_1, ..., t_{N-1} domains of ND spectrum divided by number of t_1 increments collected in 2D-RD experiment. The theoretical signal-to-noise ratio (S/N) achieved in multiple quadrature RD experiments remains the same as in their single quadrature variants. For example formally 4D technique with three chemical shifts in common dimension proposed recently by Ding and Gronenborn could be considered (Ding and Gronenborn, 2002). The analogous experiments with quadrature for all three indirectly detected frequencies would require acquisition of eight, i.e., four-fold more, data sets per t_1 increment. However, since all of these data sets are summed prior to Fourier transformation, the S/N obtained for spectra acquired in the same measurement time; i.e., with equal number of increments, the same F_1 spectral width, and adequately adjusted number of repetitions, is retained. Considering, the narrower F_1 spectral window allow-

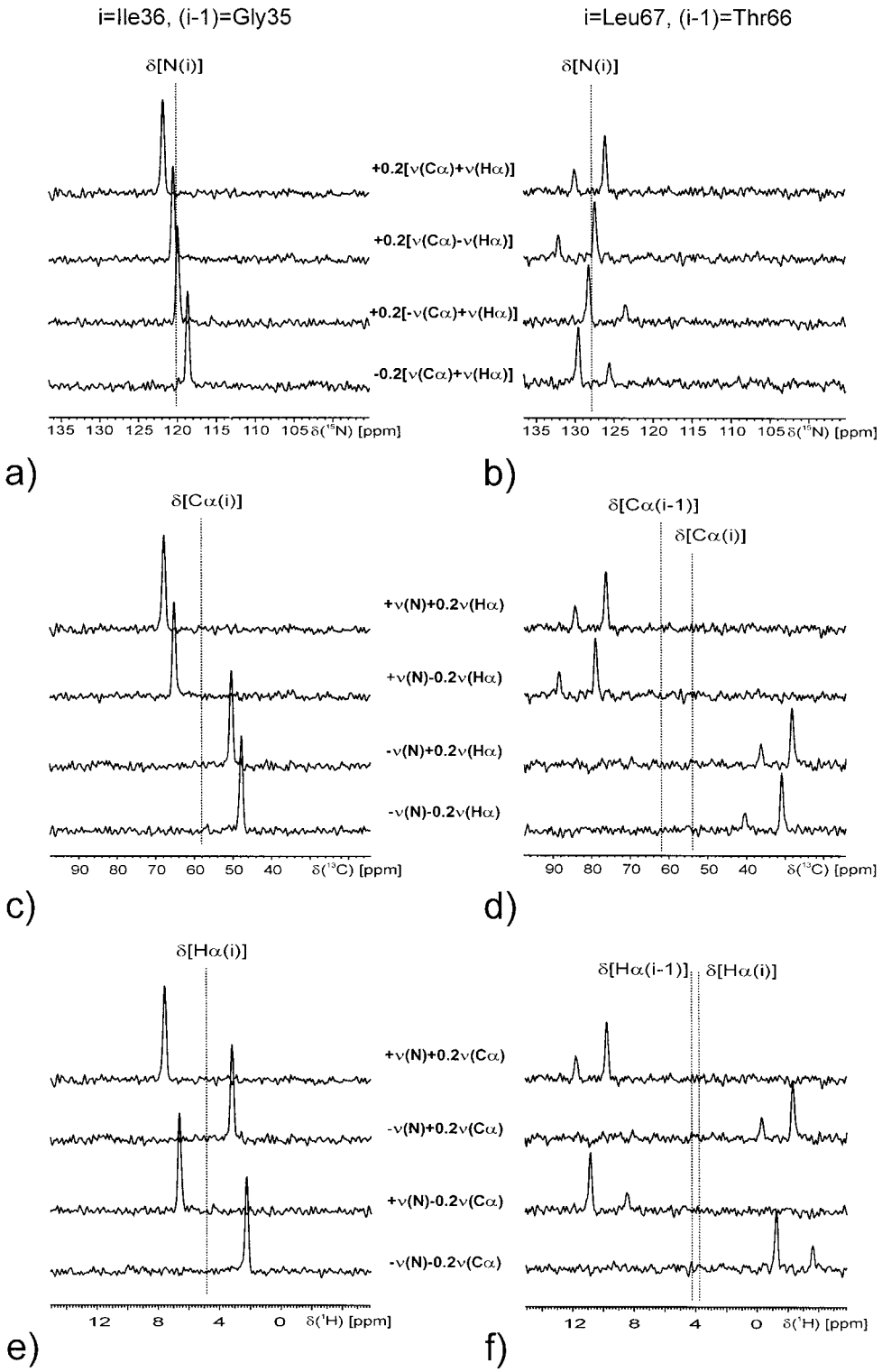

Figure 5. The F_1 traces through the Ile36 (a, c, e) and Leu67 (b, d, f) resonances, obtained from the spectra given in Figure 4. For comparison three different arrangements are shown: With positive sign of ^{15}N (a, b), $^{13}C_\alpha$ (c, d) and $^{1}H_\alpha$ (e, f) frequencies, respectively, with adequately adjusted chemical shift scale. The dotted lines indicate the chemical shifts of involved nuclei.

able in a experiments with full quadrature detection, in the same time longer evolution period can be sampled without lengthen of experiment. Although, for a very sensitive experiments and/or concentrated samples, where single scan acquisition is possible a shortest possible measurement time of multiple quadrature experiment would be four times longer, thus in such a case the Ding and Gronenborn approach could be advantageous.

Results and discussion

The 2D HNCA and 2D HN(CO)CA sequences, with simultaneously sampled $^{13}C_\alpha$ and ^{15}N chemical shift evolution, were adapted from the original 3D versions (Ikura et al., 1990; Grzesiek and Bax, 1992; Muhandiram and Kay, 1994; Kay et al., 1994; Yamazaki et al., 1994), implemented in the Varian Userlib ProteinPack package (Varian Inc., Palo Alto, 2002). Both experiments are of the out and back type and employ constant-time ^{15}N evolution. In both cases phase modulation in t_2 is obtained as a result of sensitivity enhancement detection scheme (Palmer III et al., 1991; Kay et al., 1992; Sattler et al., 1995), and it is combined with amplitude modulation in t_1, using the States-TPPI (Marion et al., 1989) method. The modification was achieved simply by setting the t_2 evolution time equal to t_1, while retaining the all statements responsible for quadrature in both evolution times. The resulting experiments produced an array of four data sets per each t_1 increment (echo- and anti-echo in respect to ^{15}N, both with sine and cosine modulation due to $^{13}C_\alpha$ frequencies), which should be acquired in interleaved mode. The processing scheme which allows one to obtain spectra with peaks at $\delta(^{15}N) + \nu(^{13}C_\alpha)$ and $\delta(^{15}N) - \nu(^{13}C_\alpha)$ is described in Table 1.

The spectra obtained using modified 2D HN(CO)CA and 2D HNCA sequences are shown in Figure 1(a, b) and (c, d), respectively. In comparison with a conventional ^1H-^{15}N HSQC experiment the cross-peak dispersion is enhanced by combination of both ^{15}N and ^{13}C frequencies in the F_1 dimension, while their number is retained. It is worth noting that the obtained signal pattern is different for the two possible combinations of the ^{15}N and ^{13}C frequencies. This could enable one to recognize and to assign peaks which are overlapped in one of the spectra. As a consequence of constant-time ^{15}N evolution, the maximum t_1 time of only 27.9 ms could be used. In the presented case this produced sufficient quality of the experiment. However, the effective resolution could be further improved using not limited by ^{15}N-^{13}C coupling refocusing period, 'real-time' or 'semi-constant-time' evolution (Sattler et al., 1999) of ^{15}N chemical shifts. In such a case the evolution of C_α coherences should be scaled down to allow full evolution of the slower relaxing ^{15}N nuclei.

Figure 2 provides two different examples of F_1 cross-sections obtained from the spectra presented in Figure 1. The ^{15}N chemical shifts are marked by dotted lines, and arrows assign the relative $^{13}C_\alpha$ frequencies. Note that the signal displacements for the Ile36 and Leu67 residues are reversed, which indicates opposite signs of the respective $^{13}C_\alpha$ frequencies. Interestingly, for all signals except the interresidual correlations involving C_α of glycine residues, the residual doublet structure due to C_α-C_β scalar coupling is recognizable. This difficult to decouple splitting decreases obtainable S/N and increases F_1 line-width. However, this feature could be useful for sequential identification of amino acid residues following Gly, and for determination of these valuable coupling magnitudes (Cornilescu et al., 2000).

The pulse sequence scheme for the HACANH experiment is depicted in Figure 3. For both the intra- and inter-residual correlations, the three H_α, C_α, and N frequencies are labeled in a common time domain, and therefore four chemical shifts could be correlated in a single 2D measurement. The sequence is designed as an $H_\alpha(i), H_\alpha(i\text{-}1) \rightarrow H_N(i)$ transfer experiment, however, it could be also considered in the out and back fashion. After the transfer of the initially excited steady-state $H_\alpha(i)$ and $H_\alpha(i\text{-}1)$ protons magnetization to the respective C_α nuclei, the H_α/C_α zero- and double-quantum coherences are created and evolve during $k*t_1$ period, taking advantage of the less effective relaxation of such coherences. The following refocused $^{13}C_\alpha - ^{15}N$ INEPT step allows creation of single quantum ^{15}N coherences, which after evolution in t_1 are transferred to amide protons H_N for detection in t_2. The factor k could be used for the relative scaling of both evolution periods in order to optimize the maximum t_1 and the expected resolution with respect to the effective transverse relaxation rates. The quadrature for ^{15}N is obtained by simultaneous inversion of ψ and G_1, while for $^{13}C_\alpha$ and $^1H_\alpha$ by States and States-TPPI incrementation of φ_2 and φ_1, respectively. Thus, for a correct result eight data sets, consisting of all possible combinations of ψ/G_1, φ_1 and φ_2, should be recorded for each t_1 increment and stored separately. Their appropriate combination as described in Table 2,

Table 1. Appropriate combination of four data sets per each t_1 increment for 2D RD-HNCA and HN(CO)CA experiments presented in this work. In both cases, amplitude modulation (sine/cosine – S/C) for ^{13}C (States-TPPI) and phase modulation for ^{15}N frequencies (echo/antiecho – E/A) is generated. R and I denotes real and imaginary parts of the successive FIDs, respectively

Data set			Modulation	Contribution to the t_1 interferogram	
	^{15}N	^{13}C		Real part	Imaginary part
1	E	C	$[\cos(\Omega_N t_1) - i\sin(\Omega_N t_1)]\cos(\Omega_C t_1)$	R	aI
2	A	C	$[\cos(\Omega_N t_1) + i\sin(\Omega_N t_1)]\cos(\Omega_C t_1)$	R	$-a$I
3	E	S	$[\cos(\Omega_N t_1) - i\sin(\Omega_N t_1)]\sin(\Omega_C t_1)$	abI	$-b$R
4	A	S	$[\cos(\Omega_N t_1) + i\sin(\Omega_N t_1)]\sin(\Omega_C t_1)$	$-ab$I	$-b$R

The a and b factors determine sign of ^{15}N and ^{13}C frequencies, respectively.
$a = -1, b = -1$ cross-peaks at $\nu(^{15}\text{N}) + \nu(^{13}\text{C})$
$a = -1, b = 1$ cross-peaks at $\nu(^{15}\text{N}) - \nu(^{13}\text{C})$
Note: The processing macros for Varian VNMR 6.1B (Varian Inc. Palo Alto) and NMRPipe (Delaglio et al., 1995) software are available from authors on request. The signs of a and b may depend on particular implementation and spectrometer type.

Table 2. Appropriate combination of eight data sets per each t_1 increment for 2D RD-HACANH experiment presented in this work (Figure 1). Amplitude modulation (sine/cosine – S/C) for ^{1}H and ^{13}C (States and States-TPPI) and phase modulation for ^{15}N frequencies (echo/antiecho –E/A) is generated. R and I denotes real and imaginary parts of the successive FIDs, respectively and k is the scaling factor

Data set				Modulation	Contribution to the t_1 interferogram	
	^{15}N	^{13}C	^{1}H		Real part	Imaginary part
1	E	C	C	$[\cos(\Omega_N t_1) - i\sin(\Omega_N t_1)]\cos(\Omega_C t_1)\cos(\Omega_H t_1)$	R	aI
2	A	C	C	$[\cos(\Omega_N t_1) + i\sin(\Omega_N t_1)]\cos(\Omega_C t_1)\cos(\Omega_H t_1)$	R	$-a$I
3	E	S	C	$[\cos(\Omega_N t_1) - i\sin(\Omega_N t_1)]\sin(\Omega_C t_1)\cos(\Omega_H t_1)$	abI	$-b$R
4	A	S	C	$[\cos(\Omega_N t_1) + i\sin(\Omega_N t_1)]\sin(\Omega_C t_1)\cos(\Omega_H t_1)$	$-ab$I	$-b$R
5	E	C	S	$[\cos(\Omega_N t_1) - i\sin(\Omega_N t_1)]\cos(\Omega_C t_1)\sin(\Omega_H t_1)$	acI	$-c$R
6	A	C	S	$[\cos(\Omega_N t_1) + i\sin(\Omega_N t_1)]\cos(\Omega_C t_1)\sin(\Omega_H t_1)$	$-ac$I	$-c$R
7	E	S	S	$[\cos(\Omega_N t_1) - i\sin(\Omega_N t_1)]\sin(\Omega_C t_1)\sin(\Omega_H t_1)$	$-bc$R	$-abc$I
8	A	S	S	$[\cos(\Omega_N t_1) + i\sin(\Omega_N t_1)]\sin(\Omega_C t_1)\sin(\Omega_H t_1)$	$-bc$R	abcI

The a, b and c factors determine sign of ^{15}N, ^{13}C and ^{1}H frequencies, respectively.
$a = 1, b = 1, c = 1$ cross-peaks at $\nu(^{15}\text{N}) + k[\nu(^{13}\text{C}) + \nu(^{1}\text{H})]$
$a = 1, b = 1, c = -1$ cross-peaks at $\nu(^{15}\text{N}) + k[\nu(^{13}\text{C}) - \nu(^{1}\text{H})]$
$a = 1, b = -1, c = 1$ cross-peaks at $\nu(^{15}\text{N}) + k[-\nu(^{13}\text{C}) + \nu(^{1}\text{H})]$
$a = 1, b = -1, c = -1$ cross-peaks at $\nu(^{15}\text{N}) + k[-\nu(^{13}\text{C}) - \nu(^{1}\text{H})]$
Note: The processing macros for Varian VNMR 6.1B (Varian Inc. Palo Alto) and NMRPipe (Delaglio et al., 1995) software are available from authors on request. The signs of a, b and c may depend on particular implementation and spectrometer type.

provides the set of four independent spectra plotted in Figure 4. Again the relative cross-peak displacements are different in each spectrum which is helpful for signal assignment. Sample F_1 traces are shown in Figure 5. It is characteristic for the discussed HACANH experiment that the signal originating from the Gly35 residue vanishes owing to the inability to refocus C-H coupling in the second Δ_1 period for the CH_2 group. A three different arrangements of spectra are shown with signal frequencies distributed around ^{15}N, ^{13}C, and ^{1}H chemical shifts.

An interesting feature of the proposed method is the excess of information obtainable for $n > 2$. The number of independent spectra which can be generated from acquired data is equal to 2^{n-1} (the number of lines in a spectrum with single quadrature). Thus, e.g., for $n = 3$, available are four independent, out of eight possible, combinations of the frequency signs, e.g. : $\Omega_A + \Omega_B + \Omega_C$, $\Omega_A - \Omega_B + \Omega_C$, $\Omega_A + \Omega_B - \Omega_C$, and $\Omega_A - \Omega_B - \Omega_C$. Hence, there are four linear equations describing three unknowns for $n = 3$, and eight equations for four unknowns for $n = 4$. Since the cross-peak displacements in all the spectra are,

in general, different, the same peaks could be overlapped in one spectrum while separated in the others, still enabling a full analysis. Additionally, the precision of obtained chemical shifts could be significantly improved by simple averaging.

In Figures 1, 2, and 4, for clarity and convenient signal frequency calculations, we decided to keep constant positive sign of ^{15}N frequencies combined with all possible combinations of the other ones. Therefore, the peaks obtained using the described data sets combination, are centered around ^{15}N frequency. However, different arrangements of the spectra are also possible as illustrated on Figure 5. Note that, due to the determination of the sign of the rotating frame frequency for all nuclei involved, the frequency offsets could be set in the center of the regions of interest, thus reducing the sampled spectral width to a minimum, i.e. the sum of the respective spectral ranges.

All the spectra presented were recorded at 298 K on a Varian Unity Plus 500 spectrometer equipped with a Performa II z-PFG unit and a 5 mm ^{1}H, ^{13}C, ^{15}N - triple resonance probehead. High power ^{1}H, ^{13}C, and ^{15}N $\pi/2$ pulses of 6.5, 14.4, and 48.0 μs, respectively, were employed. A sample of 1.5 mM ^{13}C, ^{15}N-labeled ubiquitin in 9:1 H_2O/D_2O, at pH = 6.0 was used.

Conclusions

The application of quadrature detection for all the frequencies sampled simultaneously enables full exploration of the advantages of reduced dimensionality experiments, i.e., short measurement times and the resolution limited only by apparent transverse relaxation rates. We have demonstrated that multiple quadrature detection not only clarifies the spectrum by two-fold reduction of the number of peaks for each frequency in the RD-domain, but also allows decreasing the sampled frequency range. Additionally, implementation of this technique in the existing pulse-sequences is straightforward. The described modification of the RD-techniques, due to the high resolution and the presence of redundant information, is ideally suitable for precise peak-peaking algorithms (Koradi et al., 1998) and automatic assignment of NOESY cross-peaks (Mumenthaler et al., 1997; Herrmann et al., 2002). We believe that RD-experiments with multiple quadrature detection will find a variety of applications in the field of biomolecular NMR.

Acknowledgement

The authors are grateful to Prof Andrew R. Byrd (Structural Biophysics Laboratory, National Cancer Institute-Frederick, Frederick, MD) for the sample of ^{13}C, ^{15}N-double labeled ubiquitin.

Notes

After submission of this work a similar approach has been published (Kim and Szyperski, 2003).

References

Bax, A. and Grzesiek, S. (1993) *Acc. Chem. Res.*, **26**, 131–138.
Bodenhausen G. and Ernst, R.R. (1981) *J. Magn. Reson.*, **45**, 367–373.
Bodenhausen G. and Ernst, R.R. (1982) *J. Am. Chem. Soc.*, **104**, 1304–1309.
Brutscher, B., Cordier, F., Simorre, J.P., Caffrey, M.S. and Marion, D., (1995) *J. Biomol. NMR*, **5**, 202–206.
Brutscher, B., Simorre, J.P., Caffrey, M.S. and Marion, D. (1994) *J. Magn. Reson.*, **B 105**, 77–82.
Cornilescu, G., Bax, A. and Case, D.A. (2000) *J. Am. Chem. Soc.*, **122**, 2168–2171.
Delaglio, F., Grzesiek, S., Vuister, G.W., Zhu, G., Pfeifer J. and Bax, A. (1995) *J. Biomol. NMR*, **6**, 277–293.
Ding, K. and Gronenborn, A.M. (2002) *J. Magn. Reson.*, **156**, 262–268.
Grzesiek, S. and Bax, A. (1992) *J. Magn. Reson.*, **96**, 432–440.
Herrmann, T., Güntert, P. and Wüthrich, K. (2002) *J. Mol. Biol.*, **319**, 209–227.
Ikura, M., Kay, L.E. and Bax, A. (1990) *Biochemistry*, **29**, 4659–4667.
Kay, L.E. Keifer, P. and Saarinen, T. (1992) *J. Am. Chem. Soc.*, **114**, 10663–10665.
Kay, L.E., Xu, G.Y. and Yamazaki, T. (1994) *J. Magn. Reson.*, **A 109**, 129–133.
Kim, S. and Szyperski, T. (2003) *J. Am. Chem. Soc.*, **125**, 1385–1393.
Koradi, R., Billeter, M., Engeli, M., Guntert P. and Wüthrich K., (1998) *J. Magn. Reson.*, **135**, 288–297.
Löhr, F. and Rüterjans, H. (1995) *J. Biomol. NMR*, **6**, 189–197.
Marion, D., Ikura, M., Tschudin, R. and Bax, A. (1989) *J. Magn. Reson.*, **85**, 393–399.
Montelione, G.T. and Wagner, G. (1989) *J. Am. Chem. Soc.*, **111**, 5474–5475.
Muhandiram, D.R. and Kay, L.E. (1994) *J. Magn. Reson.*, **B 103**, 203–216.
Mumenthaler, C., Güntert, P., Braun, W. and Wüthrich, K. (1997) *J. Biomol. NMR*, **10**, 351–362.
Ottiger, M., Delaglio, F. and Bax, A. (1998) *J. Magn. Reson.*, **131**, 373–376.
Palmer III, A.G., Cavanagh, J., Wright, P.E. and Rance, M. (1991) *J. Magn. Reson.*, **93**, 151–170.
Pervushin, K.V., Riek, R., Wider, G. and Wüthrich, K. (1997) *Proc. Natl. Acad. Sci. USA*, **94**, 12366–12371.
Sattler, M., Schleuchter, J. and Griesinger, C. (1999) *Prog. NMR Spectrosc.*, **34**, 93–158.

Sattler, M., Schwedinger, M.G., Schleuchter, J. and Griesinger, C. (1995) *J. Biomol. NMR*, **5**, 11–22.
States, D.J., Haberkorn, R.A. and Ruben, R.J. (1982) *J. Magn. Reson.*, **48**, 286–292.
Szyperski, T., Banecki, B., Braun, D. and Glaser, R.W. (1998) *J. Biomol. NMR*, **11**, 387–405.
Szyperski, T., Braun, D., Banecki, B. and Wüthrich, K. (1996) *J. Am. Chem. Soc.*, **118**, 8146–8147.
Szyperski, T., Braun, D., Fernández, C., Bartels, C. and Wüthrich, K. (1995) *J. Magn. Reson.*, **B 108**, 197–203.
Szyperski, T., Fernández, C. and Wüthrich, K. (1997) *J. Magn. Reson.*, **128**, 228–232.
Szyperski, T., Pellecchia, M. and Wüthrich, K. (1994) *J. Magn. Reson.*, **B 105**, 188–191.
Szyperski, T., Wider, G., Buschweller, J.H. and Wüthrich, K. (1993a) *J. Am. Chem. Soc.*, **115**, 9307–9308.
Szyperski, T., Wider, G., Bushweller, J.H. and Wüthrich, K. (1993b) *J. Biomol. NMR*, **3**, 127–132.
Weigelt, J. (1998) *J. Am. Chem. Soc.*, **120**, 16778–116779.
Wüthrich, K. (1986) *NMR of Proteins and Nucleic Acids*, John Wiley and Sons, New York, NY.
Xia, Y., Arrowsmith, C.H. and Szyperski, T. (2002) *J. Biomol. NMR*, **24**, 41–50.
Yamazaki, T., Lee, W., Arrowsmith, C.H., Muhandiram, D.R. and Kay, L.E. (1994) *J. Am. Chem. Soc.*, **116**, 11655–11666.